

**Biogeochemical
variability in the
equatorial Indian
Ocean**

P. G. Strutton et al.

Biogeochemical variability in the equatorial Indian Ocean during the monsoon transition

P. G. Strutton¹, V. J. Coles², R. R. Hood², R. J. Matear³, M. J. McPhaden⁴, and H. E. Phillips¹

¹Institute for Marine and Antarctic Studies, University of Tasmania, Hobart, Australia and Australian Research Council Centre of Excellence for Climate System Science, Hobart, Australia

²Horn Point Laboratory, University of Maryland Center for Environmental Studies, Cambridge, USA

³Commonwealth Scientific and Industrial Research Organisation, Marine and Atmospheric Research, Hobart, Australia

⁴National Oceanic and Atmospheric Administration, Pacific Marine Environmental Laboratory, Seattle, USA

Received: 15 January 2014 – Accepted: 18 January 2014 – Published: 29 April 2014

Correspondence to: P. G. Strutton (peter.strutton@utas.edu.au)

Published by Copernicus Publications on behalf of the European Geosciences Union.

Title Page

Abstract

Introduction

Conclusions

References

Tables

Figures

⏪

⏩

◀

▶

Back

Close

Full Screen / Esc

Printer-friendly Version

Interactive Discussion

Abstract

In this paper we examine time-series measurements of near-surface chlorophyll concentration from a mooring that was deployed at 80.5° E on the equator in the Indian Ocean in 2010. These data reveal at least six striking spikes in chlorophyll in October through December, with approximately 2 week periodicity, that coincide with the development of the fall Wyrтки jets during the transition between the summer and winter monsoons. Concurrent meteorological and in situ physical measurements from the mooring reveal that the chlorophyll pulses are associated with intensification of eastward winds at the surface and eastward currents in the mixed layer. These observations are inconsistent with upwelling dynamics as occurs in the Atlantic and Pacific Oceans, since eastward winds that force Wyrтки jet intensification should drive downwelling. The chlorophyll spikes could be explained by two alternative mechanisms: (1) turbulent entrainment of nutrients and/or chlorophyll from across the base of the mixed layer by wind stirring or Wyrтки jet-induced shear instability; or (2) enhanced horizontal advection of high chlorophyll concentrations into the convergent equatorial zone. The first mechanism is supported by the phasing and amplitude of the relationship between wind stress and chlorophyll, which suggests that the chlorophyll spikes are the result of turbulent entrainment driven by synoptic zonal wind events. The second mechanism is supported by satellite chlorophyll observations that reveal a clear connection between the increased chlorophyll concentrations at the mooring location and larger-scale topographic wake effects from the Chagos–Lacadvive Ridge upstream. The biweekly periodicity of the chlorophyll spikes appears to be related to the presence of mixed Rossby-gravity waves, also known as Yanai waves, which can be seen throughout the time-series as a biweekly periodicity in the meridional velocities with upward phase propagation. Consistent with hypothesis 2, eastward flows over the Chagos–Lacadvive Ridge generate high chlorophyll concentrations to the north of the equator and periodic southward advection in the meridional flows associated with Yanai waves produces the chlorophyll spikes that are observed in the mooring record. Yanai waves may also con-

BGD

11, 6185–6219, 2014

Biogeochemical variability in the equatorial Indian Ocean

P. G. Strutton et al.

Title Page

Abstract

Introduction

Conclusions

References

Tables

Figures



Back

Close

Full Screen / Esc

Printer-friendly Version

Interactive Discussion



tribute to vertical shear across the base of the mixed layer that could help support entrainment. The OFAM3 eddy-resolving model suggests that both of our proposed mechanisms may be important. Climatological satellite chlorophyll data show that the elevated chlorophyll concentrations in this region are consistently observed year after year and so are reflective of recurring large-scale wind and circulation-induced productivity enhancement in the central equatorial Indian Ocean.

1 Introduction

Although our ability to describe and model the oceans has advanced rapidly in recent decades, our understanding of the physical, biogeochemical and ecological dynamics of the Indian Ocean is still rudimentary in many respects. This is due, in part, to the fact that the Indian Ocean remains under sampled in both time and space compared to the Pacific and Atlantic. Moreover, the Indian Ocean is a dynamically complex and highly variable system under monsoonal influence. Although recent focused research in the Indian Ocean has significantly improved our ability to understand and predict physical dynamics and ocean–atmosphere interactions (Schott et al., 2009), the biogeochemical and ecological impacts of this complex physical forcing are not yet fully understood (Hood et al., 2009). This is particularly true in the equatorial zone where atmospheric forcing and the physical response have been relatively comprehensively studied, but the biogeochemical and ecological responses have not.

The equatorial Indian Ocean is strongly influenced by several different physical processes at intraseasonal and interannual time scales. These include the eastward Wyrтки jets that occur semi-annually during inter-monsoon periods (Han et al., 1999; Wyrтки, 1973); the Madden–Julian Oscillation (MJO), which is characterized by 30–60 day variability and eastward propagation of atmospheric convection cells (Madden and Julian, 1971; Hendon and Salby, 1994); and positive and negative Indian Ocean Dipole (IOD) events, where positive events exhibit unusually strong easterly equatorial winds, and anomalous upwelling in the eastern Indian Ocean (Saji et al., 1999; Vinayachan-

BGD

11, 6185–6219, 2014

Biogeochemical variability in the equatorial Indian Ocean

P. G. Strutton et al.

Title Page

Abstract

Introduction

Conclusions

References

Tables

Figures

⏪

⏩

◀

▶

Back

Close

Full Screen / Esc

Printer-friendly Version

Interactive Discussion

dran et al., 2009). Roughly 16 positive and 9 negative events occurred over the period 1950–2004 (Ihara et al., 2008).

The Wyrтки jets, which are narrow currents flowing eastward along the equator at peak speeds of $\sim 1 \text{ ms}^{-1}$ (Nagura and McPhaden, 2010a; Joseph et al., 2012), occur with regularity every boreal spring and fall, though there is significant interannual variability in their strength associated with the IOD (Schott and McCreary, 2001; Nagura and McPhaden, 2010b). The spring jet is strongest in April–May and the fall jet is strongest from late October to early December; its formation is accompanied by thermocline uplift in the western basin and by thermocline depression in the east (Wyrтки, 1973).

Wiggert et al. (2006) argued that the main biogeochemical impact of the Wyrтки jets is to depress the thermocline and nitracline on the eastern side of the basin and therefore lower equatorial primary production upon their arrival in May and November. This is consistent with a 25 day shipboard time series from the equator at 80.5° E in late 2006 that revealed deepening of the surface layer, nitracline and subsurface chlorophyll maximum during the fall Wyrтки jet period (Kumar et al., 2012). However, these data also revealed a biweekly shoaling of the lower thermocline and the depth of the chlorophyll maximum, associated with the passage of mixed Rossby-gravity waves. These waves, first observed in the atmosphere by Yanai and Maruyama (1966), are equatorially trapped planetary waves with a Gaussian structure in meridional velocity that is centered at the equator. When the phase is propagating eastward they behave like inertia-gravity waves, and they can be seen in time-series data as a biweekly periodicity in meridional velocity with upward phase propagation. There have been no studies revealing a significant biogeochemical impact from the passage of these waves in the Indian Ocean.

In an effort to obtain a better characterization of these and other kinds of atmospheric and oceanic variability in the Indian Ocean, CLIVAR (the Climate Variability and Predictability program) and GOOS (the Global Ocean Observing System) are deploying a basin-wide observing system in the Indian Ocean, called the Indian Ocean

BGD

11, 6185–6219, 2014

Biogeochemical variability in the equatorial Indian Ocean

P. G. Strutton et al.

Title Page

Abstract

Introduction

Conclusions

References

Tables

Figures

⏪

⏩

◀

▶

Back

Close

Full Screen / Esc

Printer-friendly Version

Interactive Discussion



**Biogeochemical
variability in the
equatorial Indian
Ocean**

P. G. Strutton et al.

[Title Page](#)[Abstract](#)[Introduction](#)[Conclusions](#)[References](#)[Tables](#)[Figures](#)[Back](#)[Close](#)[Full Screen / Esc](#)[Printer-friendly Version](#)[Interactive Discussion](#)

Observing System, or IndOOS (International CLIVAR Project Office, 2006). An array of 46 buoys is planned between 16° N and 26° S spanning the entire basin (the Research moored Array for African–Asian–Australian Monsoon Analysis and Prediction or RAMA; McPhaden et al., 2009). The RAMA array is 70 % complete as of December 2013.

5 These moorings are capable of measuring a broad suite of key variables needed to describe, understand and predict large-scale ocean dynamics and ocean–atmosphere interactions. They also provide an excellent atmospheric and physical oceanographic context for biogeochemical studies in the Indian Ocean.

10 In this paper we describe results from the first biogeochemical sensor deployment on a RAMA mooring, along with concurrent atmospheric, physical oceanographic and remote sensing measurements. These data reveal a series of striking chlorophyll spikes, with approximately 2 week periodicity in October through December, that are associated with the development of the fall Wyrтки jet. Chlorophyll variability of this magnitude is not found prior to the onset of the boreal autumn Wyrтки jet (May–September). Although the timing of the spikes appears to be related to local synoptic wind events and local entrainment at the equator, satellite chlorophyll observations also reveal a clear connection between the increased chlorophyll concentrations at the mooring and larger-scale topographic wake effects from the Chagos–Lacadvive Ridge up-stream. The biweekly periodicity of the chlorophyll spikes suggests a link to biweekly mixed Rossby-gravity waves. These observations, combined with insights obtained from a coupled physical-biogeochemical model, suggest that perturbations of eastward flows over the Chagos–Lacadvive Ridge generate high chlorophyll concentrations to the north of the equator and that periodic southward advection in the meridional flows associated with the passage of mixed Rossby-gravity waves produces the chlorophyll spikes observed in the mooring record. However, wind and Wyrтки jet-induced entrainment of nutrients or chlorophyll, or both, from depth may also contribute to the forcing of the spikes in chlorophyll.

15

20

25

2 Methods

2.1 RAMA mooring observations

A RAMA mooring was deployed on 22 May 2010 at 80.6° E, 0.1° N and recovered on 16 December 2010. The deployment was in oligotrophic waters about 800 km east of the potential influence of mesotrophic waters around the Maldives (73.5° E, 0.5° N), which form part of the Chagos–Lacadive Ridge.

The following moored observations are available (McPhaden et al., 2009): shortwave and longwave solar radiation measured at 3.5 m above the sea surface; rain rate measured at 3.5 m above the sea surface; wind speed and direction at 4 m above the sea surface; relative humidity measured at 3 m above the sea surface; sea-level barometric pressure and air temperature measured at 3 m above the sea surface; ocean temperature at 1 m (nominally, sea surface temperature) and at 5, 10, 13, 20, 40, 43, 60, 80, 100, 120, 140, 180, 300, 500 m below the surface; salinity at 1 m (surface salinity) and at 10, 20, 40, 60, 100 and 140 m below the surface; current speed and direction at 10 and 40 m below the surface. Some of these data were not available for the entire deployment due to sensor failure. From these observations the TAO project disseminates derived parameters, of which we use the depth of the 20 °C isotherm (m), as a proxy for thermocline depth and ADCP-derived current vectors (m s^{-1}).

In addition to the standard RAMA mooring instrumentation, a combined chlorophyll fluorescence and backscatter sensor (FLNTU) manufactured by WETLabs (Philomath, Oregon, USA) was mounted at 25 m below the surface. The FLNTU chlorophyll excitation and emission wavelengths were 470 nm and 695 nm, respectively. The backscatter wavelength was 700 nm. For the gain settings used in this deployment, variability in the backscatter channel was barely detectable, so these data will not be discussed further. Fluorescence was converted to chlorophyll concentration using:

$$\text{chl} [\text{mg m}^{-3}] = \text{scale factor} \times (\text{output} - \text{dark counts})$$

BGD

11, 6185–6219, 2014

Biogeochemical variability in the equatorial Indian Ocean

P. G. Strutton et al.

Title Page

Abstract

Introduction

Conclusions

References

Tables

Figures

⏪

⏩

◀

▶

Back

Close

Full Screen / Esc

Printer-friendly Version

Interactive Discussion

where output is the raw data from the instrument in counts, and scale factor ($0.0121 \text{ [mg m}^{-3}\text{] count}^{-1}$) and dark counts (50 counts) were from the instrument's factory calibration on 14-Oct-2009. This equation resulted in one negative daily mean chlorophyll concentration for the period of the deployment, so the dark count value was adjusted to 45 counts, bringing the time series of FLNTU chlorophyll into closer agreement with the satellite chlorophyll estimates from the vicinity of the mooring. Although this conversion from fluorescence to chlorophyll is only semi-quantitative, we are less concerned with the accuracy of the chlorophyll measurements than we are with their temporal variability. Optical instruments are subject to fouling, which we usually diagnose as an increase in the baseline value, or noisy variability of the fluorescence or backscatter channels, or both. There was no increase in the baseline fluorescence values although there was an increase in variability of the fluorescence channel (the chlorophyll spikes). This variance was periodic rather than noisy, which we interpret as real environmental variability. The mooring-observed increase in fluorescence variability is also confirmed by satellite chlorophyll observations.

We use the RAMA mooring data to investigate physical mechanisms driving chlorophyll variability at the mooring. Lagged correlations between the following pairs of parameters were calculated:

1. Wind speed and temperature at 20 m.
2. Wind speed and chlorophyll at 25 m.
3. Zonal current speed (u) at 10 m and chlorophyll at 25 m.
4. Meridional current speed (v) at 10 m and chlorophyll at 25 m.
5. Temperature at 20 m and chlorophyll at 25 m.
6. Salinity at 40 m and chlorophyll at 25 m.

In addition, we also computed the autocorrelation function of chlorophyll at 25 m.

BGD

11, 6185–6219, 2014

Biogeochemical variability in the equatorial Indian Ocean

P. G. Strutton et al.

[Title Page](#)

[Abstract](#)

[Introduction](#)

[Conclusions](#)

[References](#)

[Tables](#)

[Figures](#)

[⏪](#)

[⏩](#)

[◀](#)

[▶](#)

[Back](#)

[Close](#)

[Full Screen / Esc](#)

[Printer-friendly Version](#)

[Interactive Discussion](#)

In the results section we summarize these correlations and their lags, and use them to build a conceptual model of the physical drivers that lead to the increased chlorophyll in the second half of 2010, including the regular peaks observed. We also performed the same cross-correlation analyses with model output.

2.2 Satellite observations

Satellite chlorophyll observations from both the Sea-viewing Wide Field-of-view Sensor (SeaWiFS) and the MODerate resolution Imaging Spectroradiometer (MODIS Aqua) were used to quantify the spatial and temporal chlorophyll variability in the vicinity of the mooring. To quantify the climatological seasonal cycle of chlorophyll in a 1° latitude by 1° longitude box centered on the mooring, all available 8 day average, 9 km SeaWiFS and MODIS data from 1 January 1998 to 31 December 2012 were averaged. This means that when both sensors were operating simultaneously, the two were averaged. This was the case most of the time from mid 2002 to late 2010. Similar time series of both 8 day and daily data were extracted for just 2010, for direct comparison with the moored fluorescence time series. We acknowledge possible differences between SeaWiFS and MODIS chlorophyll measurements, but chose to average across sensors to increase spatial and temporal coverage in this cloudy environment.

MODIS seasonal climatologies of sea surface temperature (SST) were obtained from NASA to depict the seasonal cycle for the central Indian Ocean. NOAA Optimum Interpolation (OI) version 2, daily SST data were used for producing a Hovmuller plot for 2010. Likewise, Hovmuller plots of sea surface height anomaly (SSHA) and surface winds were produced from weekly Archiving, Validation and Interpretation of Satellite Oceanographic data (AVISO) mean sea level anomaly data and daily WindSat acquired from Remote Sensing Systems, respectively. Currents were obtained from the OSCAR project (Ocean Surface Current Analysis Real-time). These data are surface current speed and direction derived from altimetry and scatterometry, and were used to produce animations for comparison with surface chlorophyll patterns.

BGD

11, 6185–6219, 2014

Biogeochemical variability in the equatorial Indian Ocean

P. G. Strutton et al.

[Title Page](#)

[Abstract](#)

[Introduction](#)

[Conclusions](#)

[References](#)

[Tables](#)

[Figures](#)

[⏪](#)

[⏩](#)

[◀](#)

[▶](#)

[Back](#)

[Close](#)

[Full Screen / Esc](#)

[Printer-friendly Version](#)

[Interactive Discussion](#)



2.3 CARS and RG-Argo climatologies

The CSIRO Atlas of Regional Seas (CARS) is a gridded climatology of temperature, salinity, oxygen, nitrate, phosphate and silicate (Ridgway et al., 2002). The data used in the mapping include Argo data up to May 2009, and historical CTD and bottle data collected between 1950 and 2008. Horizontal grid spacing is 0.5° in latitude and longitude, and the data are mapped onto 79 depth levels between the surface and 5500 m. The seasonal cycle in the climatology is fit with a sine and cosine wave to generate a full annual cycle. The oxygen and nutrient data that inform the climatology are patchy in space and time in some parts of the ocean. At our mooring location this issue is minimized by the close proximity of the WOCE 18 repeat hydrography line. We used CARS 2009 to depict the seasonal cycle of salinity and nitrate with depth.

The Roemmich–Gilson Argo Climatology (RG-Argo) maps the temperature and salinity fields of Argo data from 2004 to 2011 into a monthly gridded product with grid spacing of 0.5° in latitude and longitude, over 58 pressure levels from the surface to 1975 dbar (Roemmich and Gilson, 2009). We used this climatology and Argo data from individual floats in the vicinity of the mooring to describe the mean seasonal cycle of salinity with depth and also the 2010 time-depth variability.

2.4 Biogeochemical modeling

OFAM3 (Ocean Forecasting Australia Model, version 3) is a near-global, eddy-resolving, z^* configuration of version 4.1 of the Modular Ocean Model (Griffies, 2009), developed principally for hindcasting and forecasting upper ocean conditions in non-polar regions. The key features of OFAM3 are described here, and a comprehensive technical description of OFAM3 is given in Oke et al. (2013). The model grid has 0.1° latitude and longitude grid spacing between 75° S and 75° N, with 5 m vertical resolution down to 40 m depth and 10 m vertical resolution to 200 m depth.

OFAM3 uses the vertical mixing scheme described by Chen et al. (1994), and a bi-harmonic Smagorinsky viscosity scheme described by Griffies and Hallberg (2000).

BGD

11, 6185–6219, 2014

Biogeochemical variability in the equatorial Indian Ocean

P. G. Strutton et al.

Title Page

Abstract

Introduction

Conclusions

References

Tables

Figures

◀

▶

◀

▶

Back

Close

Full Screen / Esc

Printer-friendly Version

Interactive Discussion

The model is forced with 1.5° resolution, 3 hourly surface heat, freshwater, and momentum fluxes from ERA-Interim (Dee and Uppala, 2009). Surface temperature and salinity are restored to monthly averaged observations with a restoring timescale of 10 and 30 days, respectively.

5 OFAM3 includes a biogeochemical cycling model, called the Whole Ocean Model with Biogeochemistry and Trophic-dynamics (WOMBAT). WOMBAT is a three-dimensional NPZD (nutrient, phytoplankton, zooplankton, detritus) model described by Kidston et al. (2011), with the addition of iron. In WOMBAT, phytoplankton growth is limited by light, phosphate and iron, with the minimum of these three terms limiting
10 growth.

The model was initialized at rest, with potential temperature, salinity and biophysical fields from observational-based climatologies (Oke et al., 2013) and then integrated for 32 years, including an initial 14 year spin-up period followed by 18 years simulation spanning the 1993–2010 period. We present results from 2010.

15 3 Results

3.1 Spatial context

Figure 1 shows the seasonal variability in SST, surface salinity and surface chlorophyll for a large region encompassing the mooring on the equator at 80.5° E. Sri Lanka and the southern tip of India are in the central north of each panel. On the eastern edge of each panel is Sumatra. The Maldives are just north of the equator at about 73.5° E. In the Northern Hemisphere (boreal) winter, the Arabian Sea and Bay of Bengal are relatively cool, and warm SSTs spread from Sumatra, linking the central Indian Ocean with the Indonesian warm pool (Fig. 1a). The Bay of Bengal is relatively fresh and the high salinity waters of the Arabian Sea are confined to the northwest Indian Ocean (Fig. 1b).
20 Low chlorophyll concentrations span most of the equatorial Indian Ocean and the predominantly westward surface currents are visible as a wake of elevated chlorophyll to
25

Biogeochemical variability in the equatorial Indian Ocean

P. G. Strutton et al.

Title Page

Abstract

Introduction

Conclusions

References

Tables

Figures

⏪

⏩

◀

▶

Back

Close

Full Screen / Esc

Printer-friendly Version

Interactive Discussion



the west of the Maldives (Fig. 1c). SSTs become even warmer in boreal spring, and waters of about 30 °C span the entire equatorial Indian Ocean (Fig. 1d). The Bay of Bengal remains fresh but the salty waters of the western Indian Ocean are expanding eastward and southward with a pronounced equatorial tongue of higher salinity (Fig. 1e). Basin-wide chlorophyll concentrations remain low and the higher chlorophyll around the Maldives has largely disappeared (Fig. 1f). In boreal summer, monsoonal wind mixing cools SSTs in the Arabian Sea and Bay of Bengal, while in the southern Indian Ocean, the Southern Hemisphere winter also cools the temperate and subtropical ocean (Fig. 1g). The western Indian Ocean becomes more broadly saline and the western Bay of Bengal becomes slightly saltier than in spring (Fig. 1h). The elevated productivity from the Arabian Sea upwelling system is visible in the far northwest of this region, as is elevated chlorophyll around Sri Lanka and the southern tip of India (Fig. 1i). This is around the time that chlorophyll concentrations at our RAMA mooring site began to increase (Fig. 2). In boreal autumn the warmer SSTs along the equator begin to expand poleward (Fig. 1j), the highest salinity water from the Arabian Sea is closest to the mooring site (Fig. 1k) and there is clear evidence for high chlorophyll from around the Maldives being advected eastward towards, but just north of the mooring (Fig. 1l).

3.2 Mooring time series

The time series of chlorophyll measured by the FLNTU on the mooring is shown in Fig. 2, along with satellite-derived time series for 2010 and the satellite-based climatology. The main feature of note in the FLNTU data is the increase in mean chlorophyll concentration and its temporal variability beginning in October. The 2010 satellite data are shown at two temporal resolutions: the standard 8 day NASA product (filled black circles) and a 3 day running mean of daily data (red line). For the climatology, the broadening of the standard deviation envelope suggests that the increases in both the mean chlorophyll and its variability in the latter part of 2010 are regular features at this location.

Biogeochemical variability in the equatorial Indian Ocean

P. G. Strutton et al.

Title Page

Abstract

Introduction

Conclusions

References

Tables

Figures



Back

Close

Full Screen / Esc

Printer-friendly Version

Interactive Discussion



**Biogeochemical
variability in the
equatorial Indian
Ocean**

P. G. Strutton et al.

[Title Page](#)[Abstract](#)[Introduction](#)[Conclusions](#)[References](#)[Tables](#)[Figures](#)[Back](#)[Close](#)[Full Screen / Esc](#)[Printer-friendly Version](#)[Interactive Discussion](#)

Figure 3 puts the chlorophyll time series in perspective with the physical data collected at the mooring. Over the boreal summer to winter period, the low frequency variability in the equatorial winds measured at the mooring location (Fig. 3a) is dominated by a general increase in the zonal wind beginning in mid-September. This increase is associated with the development of the Wyrтки jets (Schott and McCreary, 2001). A small tendency towards southward flow is also observed at this time in the meridional winds. An increase in zonal currents in the upper 100 m (the Wyrтки jets, Fig. 3b) is evident in response to the increasing zonal wind speed, and this eastward flow gradually deepens from mid-September to December. Meridional velocity is characterized by an approximately two week periodicity with upward phase propagation that is particularly evident from August through November (Fig. 3c). This biweekly periodicity in the meridional velocities with upward phase propagation indicates the presence of mixed Rossby-gravity waves (Kumar et al., 2012). These waves are present throughout the year and also at other equatorial moorings.

The second, third and fourth peaks in chlorophyll (Fig. 3d) coincide with the surface expression of these vertically propagating features in the meridional velocity field through mid-November. Subsequently there is a shift to more persistent southward flow between 30 m and 100 m. During the transition from boreal summer to winter, surface temperature cools and the near-surface isotherms spread (Fig. 3e). Near-surface salinity, which decreased from June to mid-July, increases from mid August through to mid-November, and then begins to decrease again (Fig. 3f).

The cross correlation plots in Fig. 4 are used to reveal potential drivers of the increased chlorophyll concentrations. The correlation analysis was performed only for the period 15 September 2010 to 15 December 2010, when the peaks in chlorophyll are observed. The chlorophyll autocorrelation peak at zero days lag is quite sharp (Fig. 4a), indicating that the peaks last for only a few days. There is a small positive but not statistically significant correlation at about 2 weeks. The cross-correlations between wind and chlorophyll, and temperature and chlorophyll (Fig. 4b) show that increased winds lead both cooler temperature and increased chlorophyll by about 3 days. This could be

indicative of mixing or entrainment from below which we will discuss later. The correlations between currents and chlorophyll (Fig. 4c) reveal no significant relationship for zonal currents, but a broad peak of negative correlation around zero days for meridional currents and chlorophyll. Finally, Fig. 4d shows that cool temperatures are correlated with higher chlorophyll around zero lag, but there is no significant correlation between salinity and chlorophyll.

3.3 Satellite and Argo analysis

The Hovmuller plot (Fig. 5) indicates that at least four, perhaps five of the chlorophyll peaks (numbered) were associated with chlorophyll signals propagating from west to east. However, the propagation was only observed in chlorophyll, and not in SST, SSH or winds. The five peaks occur around 6 October, 20 October, 1 November, 8 November and 25 November (Fig. 5e). In Fig. 5d, the 0.15 mg m^{-3} chlorophyll contour is identified to make these propagating signals more obvious. Black lines are drawn through the centers of the elevated chlorophyll contours to estimate the propagation speed. The mean propagation speed of these five chlorophyll features was $1.95 \pm 0.33 \text{ m s}^{-1}$. Unlike the chlorophyll patterns, there is no corresponding west to east signal that could be identified in contours of the 28.5°C isotherm (Fig. 5a), the 8 m s^{-1} wind contour (Fig. 5c) or by eye in the SSH plot (Fig. 5b).

The Hovmuller plots (Fig. 5) and an animation of satellite chlorophyll and OSCAR current velocities for the region (see Supplement animation chl_oscar.m4v) suggest that advection of chlorophyll from north of the mooring may be important in the formation of the chlorophyll peaks at the equator. This advection is illustrated in Fig. 6, which is a snapshot from the chlorophyll animation for 6 October 2010 with surface geostrophic currents derived from sea surface height data superimposed. The chlorophyll data shown are a 15 day average centered on 6 October, with 5 day average vectors centered on 1 October from the OSCAR product. The Maldives and the Chagos–Lacadive ridge are in a north-south line at approximately 73°E . It is clear that high chlorophyll is being generated in the region of the Maldives, and the patterns indicate

BGD

11, 6185–6219, 2014

Biogeochemical variability in the equatorial Indian Ocean

P. G. Strutton et al.

Title Page

Abstract

Introduction

Conclusions

References

Tables

Figures

⏪

⏩

◀

▶

Back

Close

Full Screen / Esc

Printer-friendly Version

Interactive Discussion



sweeping of that feature towards the equator. Note also the meridional meandering that is apparent in the current field, suggesting the presence of mixed Rossby-gravity waves.

The seasonal cycle of surface salinity (Fig. 1) and the time series of salinity observed at the mooring site (Fig. 3) indicate the arrival of high salinity water at the mooring with the onset of the fall Wyrтки Jets. To determine whether or not this is a regular feature, we examined the salinity fields in the CARS and RG-Argo atlases. Figure 7 shows time-depth sections of salinity from the CARS long-term mean, and from RG-Argo for 2010 and for the 8-year average 2004–2011. These plots clearly show elevated salinity in the latter part of the calendar year between 25 and 125 m, overlying lower salinity water that persists year-round. In CARS, the surface water remains fresh during the arrival of the subsurface salinity peak. In RG-Argo, high salinities reach the surface in November in all years, and in October as well in 2010. The high salinity waters are more saline in RG-Argo than in CARS, and are more saline in 2010 compared with the 8-year average of RG-Argo. Since there is fresh water below the high salinity layer, this suggests that horizontal advection brings the high salinity water at thermocline depth, likely sourced from the western and/or northwestern parts of the basin (Fig. 1k), and that it is entrained into the mixed layer by local wind-generated turbulence. Associated with the arrival of high salinity water and with the onset of both the spring and fall Wyrтки Jets, the nitricline in CARS also shoals. The timing of the high salinity at the mooring, coinciding with the elevated chlorophyll at the mooring implicates both advection of water from the west by Wyrтки jets and entrainment by local mixing.

4 Discussion

Based on the patterns in the data, and incorporating some model results, we evaluate two hypotheses to explain the chlorophyll spikes from October to December 2010, namely:

BGD

11, 6185–6219, 2014

Biogeochemical variability in the equatorial Indian Ocean

P. G. Strutton et al.

Title Page

Abstract

Introduction

Conclusions

References

Tables

Figures

⏪

⏩

◀

▶

Back

Close

Full Screen / Esc

Printer-friendly Version

Interactive Discussion

Biogeochemical variability in the equatorial Indian Ocean

P. G. Strutton et al.

[Title Page](#)

[Abstract](#)

[Introduction](#)

[Conclusions](#)

[References](#)

[Tables](#)

[Figures](#)



[Back](#)

[Close](#)

[Full Screen / Esc](#)

[Printer-friendly Version](#)

[Interactive Discussion](#)

1. Enhanced horizontal advection brings high chlorophyll concentrations, generated near the Maldives, into the convergent equatorial zone from the north.
2. Wind and Wyrтки jet-induced shear across the base of the mixed layer favors entrainment of nutrients and/or chlorophyll from depth.

5 With the data available it is not possible to eliminate either hypothesis, and likely both processes are acting independently and in tandem.

4.1 Evaluation of hypotheses based on observations

The feature that we are most interested in explaining is the series of spikes in the moored chlorophyll record from September through December 2010 (Fig. 2). These spikes are also partly visible in the daily satellite chlorophyll data, although gaps due to clouds prohibit the daily satellite observations from more accurately capturing the variability. As we go to 8 day averaged satellite chlorophyll, the spikes are barely evident. However, an important distinction between the in situ and satellite based chlorophyll estimates is that the 8 day satellite data show higher baseline chlorophyll concentrations suggesting a driving process that occurs relatively consistently over the time period. In contrast, the in situ measurements show little to no increase in the baseline low chlorophyll values over October to December compared to June through October. The consistent baseline indicates there was no bio-fouling of the fluorometer during this period. It also indicates that the chlorophyll variability that gives rise to elevated mean values is associated with distinct event forcing that does not persist between events. Therefore the difference between the mooring and 8 day satellite data is due to the averaging.

The right hand column of Fig. 1, and the snapshot of chlorophyll in Fig. 6 both clearly show that the interaction of the large-scale flow with the Chagos–Lacative Ridge generates high chlorophyll that is advected towards the east in the second half of the calendar year. During boreal winter the advection of high chlorophyll is to the west and the spring seems to be a period of transition. Island effects such as this are commonly

**Biogeochemical
variability in the
equatorial Indian
Ocean**

P. G. Strutton et al.

[Title Page](#)[Abstract](#)[Introduction](#)[Conclusions](#)[References](#)[Tables](#)[Figures](#)[Back](#)[Close](#)[Full Screen / Esc](#)[Printer-friendly Version](#)[Interactive Discussion](#)

observed in other parts of the world, such as in the wake of the Galapagos and Marquesas Islands in the Pacific (Legeckis et al., 2004) and Kerguelen and Crozet Islands in the Southern Ocean (Blain et al., 2007). The stimulation of chlorophyll occurs because the passage of the currents past an obstacle induces vertical and horizontal mixing, and in the Pacific and Southern Ocean examples just mentioned, the crustal material of the islands acts as a source of the limiting nutrient iron to the surface ocean.

However, two lines of evidence suggest that the pulses of high chlorophyll observed at the mooring are not simply advected from the vicinity of the Maldives. The first is the time required for a water parcel to move from the Maldives at 73.25° E to the mooring at 80.5° E, a distance of 805 km. In the Hovmuller diagram (Fig. 5) five of the six chlorophyll peaks were identified, and a line drawn through each of them. The slope of each line was calculated and converted into a mean propagation speed of $1.95 \pm 0.33 \text{ m s}^{-1}$. Is it feasible that local currents could advect high chlorophyll features at this speed? Schott and McCreary (2001, their Fig. 22) observed eastward velocities as high as 1.5 m s^{-1} in early November 1993, but most of the time the speed of the Wyrki jets was 1 m s^{-1} or less. Mean zonal and meridional velocities at 10 m at the mooring during the time periods of the four chlorophyll peaks were 0.97 and -0.29 m s^{-1} respectively (Fig. 3). Including only the upper quartile of velocity events over this period increases average zonal current speed to 1.2 m s^{-1} , which is still too slow. Therefore, we conclude that the observed velocities both during our deployment and in previous studies are almost half what they would need to be for the propagating chlorophyll features initiated at the Maldives to be advected to the mooring. The second line of evidence arguing against simply eastward propagation of the island wake high chlorophyll into the vicinity of the mooring is that the Maldives and the trailing high chlorophyll occur slightly north of the equator. We require a mechanism that moves the high chlorophyll southwards to the equator. We now explore wave processes that might be responsible for this southward advection.

The association of the chlorophyll peaks with a southward meridional flow (Fig. 4c) rules out Kelvin waves as a source since they are associated with zero meridional

phyll peaks (Fig. 5c and e). However, local stirring associated with wind mixing cannot explain the propagation of the anomalies from the Maldive ridge. That is, the wind bursts do not propagate, and in the case of peak 2, there is only a very small wind perturbation.

4.2 Evaluation of hypotheses based on model results

To help assess the two hypotheses and provide some spatial perspective to our analysis we use the OFAM3 simulations described in the methods and in Oke et al. (2013). To assess the realism of the simulation we compare it to the observations from the mooring site shown in Fig. 3. The simulated current structure in the upper ocean is similar to the observations (Fig. 9). With the onset of the wind bursts in mid-September a strong eastward current develops in the upper 100 m, which accelerates during wind bursts, consistent with the observations. For the meridional currents, southward sub-surface flow develops around 80 m in both October and November, which shoals with time consistent with, yet weaker than the observations. As discussed, such behavior is consistent with propagating Yanai waves. The simulation shows that in the upper 30 m the flow is generally northward during the September to December period but there are short periods when surface flow either weakens or reverses.

For temperature in the model and in the observations, the surface water cools over the latter half of 2010 with a layer of well mixed temperatures deepening from 60 to 80 m over the September to December period. For salinity, the simulated surface water gets saltier and a sub-surface salinity maximum develops around 100 m from mid October onward. Both features are evident in the observations (Fig. 3). Given that the model's physical behavior at the mooring site reflects many of the features evident in the observations, we were motivated to use the model to investigate the phytoplankton response observed at the mooring site.

Modeled phytoplankton concentrations at the mooring site are generally too high and with different character compared to the spikey features observed in the mooring data. This partly reflects the simulation having too much nitrate (and other nutrients) in the

BGD

11, 6185–6219, 2014

Biogeochemical variability in the equatorial Indian Ocean

P. G. Strutton et al.

Title Page

Abstract

Introduction

Conclusions

References

Tables

Figures

⏪

⏩

◀

▶

Back

Close

Full Screen / Esc

Printer-friendly Version

Interactive Discussion



plankton variability. Both the variability and the shoaling patterns in meridional velocity suggest that Yanai waves are present in the simulation.

The simulations reveal the mooring is located in a complex environment where both enhanced vertical mixing associated with westerly wind bursts and north-south excursions associated with Yanai waves play a role in the phytoplankton variability. Additional observations to the north and south of the mooring are needed to determine which mode is dominating the phytoplankton variability.

5 Conclusions

Time series measurements of near-surface chlorophyll concentration from a mooring that was deployed at 80.5° E on the equator in the Indian Ocean in 2010 reveal several striking spikes in chlorophyll in October through December, with approximately 2 week periodicity, that are associated with the development of the fall Wyrтки jet. Climatological satellite chlorophyll data show that the elevated chlorophyll concentrations and spikes in this region are consistently observed year after year and so are reflective of recurring large-scale circulation-induced productivity enhancement in the central equatorial Indian Ocean. These elevated chlorophyll concentrations are observed in spite of mean downwelling conditions, which in previous modeling studies have been associated with lower productivity. Satellite chlorophyll data also reveal increases in chlorophyll concentration north of the mooring location in October through December caused by the interaction of the large-scale zonal currents with the Chagos–Lacadeive Ridge and island wake effects. Our analysis suggests that the strong temporal variability in chlorophyll concentrations at the mooring location on the time scale of weeks is caused, at least in part, by periodic meridional (southward) advection of this large island wake-induced chlorophyll feature by Yanai waves that propagate from west to east along the equator with average speeds on the order of 1.8 m s^{-1} . In addition, there is evidence suggesting that some fraction of the observed chlorophyll variability is the result of local entrainment that is driven by synoptic zonal wind events. How-

BGD

11, 6185–6219, 2014

Biogeochemical variability in the equatorial Indian Ocean

P. G. Strutton et al.

Title Page

Abstract

Introduction

Conclusions

References

Tables

Figures

⏪

⏩

◀

▶

Back

Close

Full Screen / Esc

Printer-friendly Version

Interactive Discussion



Biogeochemical variability in the equatorial Indian Ocean

P. G. Strutton et al.

Title Page

Abstract

Introduction

Conclusions

References

Tables

Figures



Back

Close

Full Screen / Esc

Printer-friendly Version

Interactive Discussion

ever, this local mechanism cannot explain the rapid eastward propagation of elevated chlorophyll that is observed in longitude-time Hovmuller diagrams. Simulations using an eddy-resolving coupled physical-biological model indicate that both wind-driven and remote Yanai wave forcing mechanisms are important. Our results both reveal and help to explain biogeochemical variability in a poorly-understood part of the global ocean. However, additional observations are needed to fully quantify the relative importance of local vs. remote forcing mechanisms.

It will be important to better understand the generation of these large chlorophyll features, because of their differing implications for basin biogeochemistry and primary production. If equatorial chlorophyll spikes are due to Yanai waves moving a meridional chlorophyll gradient across the equator, then there is no new primary production or carbon export associated with these large features. However, if the chlorophyll spikes are generated as a result of vertical mixing and entrainment, then they represent a source of primary productivity in an otherwise oligotrophic region, and may have implications for carbon export and fisheries.

Supplementary material related to this article is available online at
<http://www.biogeosciences-discuss.net/11/6185/2014/bgd-11-6185-2014-supplement.zip>.

Acknowledgements. PS is supported by the Australian Research Council's Future Fellow scheme and the Centre of Excellence for Climate System Science. HP is supported by the Australian Research Council's Discovery Project scheme and the Centre of Excellence for Climate System Science. RM is supported by the CSIRO Wealth from Oceans National Flagship. MM is supported by NOAA. This is NOAA/PMEL contribution number 4113.

References

Blain, S., Queguiner, B., Armand, L., Belviso, S., Bombled, B., Bopp, L., Bowie, A., Brunet, C., Brussaard, C., Carlotti, F., Christaki, U., Corbiere, A., Durand, I., Ebersbach, F., Fuda, J.-L., Garcia, N., Gerringa, L., Griffiths, B., Guigue, C., Guillerm, C., Jacquet, S., Jeandel, C.,

Biogeochemical variability in the equatorial Indian Ocean

P. G. Strutton et al.

[Title Page](#)

[Abstract](#)

[Introduction](#)

[Conclusions](#)

[References](#)

[Tables](#)

[Figures](#)

[⏪](#)

[⏩](#)

[◀](#)

[▶](#)

[Back](#)

[Close](#)

[Full Screen / Esc](#)

[Printer-friendly Version](#)

[Interactive Discussion](#)

Laan, P., Lefevre, D., Lomonaco, C., Malits, A., Mosseri, J., Obernosterer, I., Park, Y.-H., Picheral, M., Pondaven, P., Remeny, T., Sandroni, V., Sarthou, G., Savoye, N., Scouarnec, L., Souhaut, M., Thuiller, D., Timmermans, K., Trull, T., Uitz, J., van-Beek, P., Veldhuis, M., Vincent, D., Viollier, E., Vong, L., and Wagener, T.: Effect of natural iron fertilisation on carbon sequestration in the Southern Ocean, *Nature*, 446, 1070–1074, 2007.

Chatterjee, A., Shankar, D., McCreary, J. P., and Vinayachandran, P. N.: Yanai waves in the western equatorial Indian Ocean. *J. Geophys. Res.-Oceans*, 118, 1556–1570, 2013.

Chen, D., Rothstein, L. M., and Busalacchi, A. J.: A hybrid vertical mixing scheme and its application to tropical ocean models, *J. Phys. Oceanogr.*, 24, 2156–2179, 1994.

Dee, D. P. and Uppala, S.: Variational bias correction of satellite radiance data in the ERA-Interim reanalysis, *Q. J. Roy. Meteor. Soc.*, 135, 1830–1841, doi:10.1002/qj.493, 2009.

Griffies, S. M.: Elements of MOM4p1, GFDL Ocean Group Technical Report 6, NOAA/Geophysical Fluid Dynamics Laboratory, Princeton, New Jersey, 444 pp., 2009.

Griffies, S. M. and Hallberg, R. W.: Biharmonic friction with a Smagorinsky-like viscosity for use in large-scale eddy-permitting ocean models, *Mon. Weather Rev.*, 128, 2935–2946, 2000.

Han, W., McCreary, J. P., Anderson, D. L. T., and Mariano, A. J.: Dynamics of the eastern surface jets in the equatorial Indian Ocean, *J. Phys. Oceanogr.*, 29, 2191–2209, 1999.

Hendon, H. H. and Salby, M. L.: The life cycle of the Madden–Julian Oscillation, *J. Atmos. Sci.*, 51, 2225–2237, 1994.

Hood, R. R., Wiggert, J. D., and Naqvi, S. W. A.: Indian Ocean Research: opportunities and challenges, in: *Indian Ocean Biogeochemical Processes and Ecological Variability*, AGU Monograph Series, American Geophysical Union, Washington DC, 409–429, 2009.

Ihara, C., Kushnir, Y., and Cane, M. A.: Warming trend of the Indian Ocean SST and Indian Ocean dipole from 1880 to 2004, *J. Climate* 21, 2035–2046, doi:10.1175/2007JCLI1945.1, 2008.

International CLIVAR Project Office: Understanding the role of the Indian Ocean in the climate system – implementation plan for sustained observations, CLIVAR Publication Series, 100, Southampton, UK, 2006.

Joseph, S., Wallcraft, A. J., Jensen, T. G., Ravichandran, M., Shenoi, S. S. C., and Nayak, S.: Weakening of spring Wyrтки jets in the Indian Ocean during 2006–2011, *J. Geophys. Res.*, 117, C04012, doi:10.1029/2011JC007581, 2012.

Biogeochemical variability in the equatorial Indian Ocean

P. G. Strutton et al.

[Title Page](#)

[Abstract](#)

[Introduction](#)

[Conclusions](#)

[References](#)

[Tables](#)

[Figures](#)

[⏪](#)

[⏩](#)

[◀](#)

[▶](#)

[Back](#)

[Close](#)

[Full Screen / Esc](#)

[Printer-friendly Version](#)

[Interactive Discussion](#)



Kidston, M., Matear, R., and Baird, M. E.: Parameter optimisation of a marine ecosystem model at two contrasting stations in the Sub-Antarctic zone, *Deep-Sea Res. Pt. II*, 58, 2301–2315, 2011.

Legeckis, R., Brown, C. B., Bonjean, F., and Johnson, E. S.: The influence of tropical instability waves and phytoplankton blooms in the wake of the Marquesas Islands during 1998 and on the currents observed during the drift of the Kon-Tiki in 1947, *Geophys. Res. Lett.*, 31, L23307, 1–4, 2004.

Madden, R. A. and Julian, P. R.: Detection of a 40–50 day oscillation in the zonal wind field in the tropical Pacific, *J. Atmos. Sci.*, 28, 702–708, 1971.

McPhaden, M. J., Meyers, G., Ando, K., Masumoto, Y., Murty, V. S. N., Ravichandran, M., Syamsudin, F., Vialard, J., Yu, L., and Yu, W.: RAMA: the research moored array for African–Asian–Australian monsoon analysis and prediction, *B. Am. Meteorol. Soc.*, 90, 459–480, 2009a.

McPhaden, M. J., Meyers, G., Ando, K., Masumoto, Y., Murty, V. S. N., Ravichandran, M., Syamsudin, F., Vialard, J., Yu, L., and Yu, W.: Supplement to RAMA: the research moored array for African–Asian–Australian monsoon analysis and prediction, *B. Am. Meteorol. Soc.*, 90, ES5–ES8, 2009b.

Miyama, T., McCreary, J. P., Sengupta, D., and Senan, R.: Dynamics of biweekly oscillations in the equatorial Indian Ocean. *J. Phys. Oceanogr.*, 36, 827–846, 2006.

Nagura, M. and M. J. McPhaden: Wyrтки Jet dynamics: seasonal variability, *J. Geophys. Res.*, 115, C07009, doi:10.1029/2009JC005922, 2010a.

Nagura, M. and M. J. McPhaden: Dynamics of zonal current variations associated with the Indian Ocean dipole, *J. Geophys. Res.*, 115, C11026, doi:10.1029/2010JC006423, 2010b.

Oke, P. R., Griffin, D. A., Schiller, A., Matear, R. J., Fiedler, R., Mansbridge, J., Lenton, A., Cahill, M., Chamberlain, M. A., and Ridgway, K.: Evaluation of a near-global eddy-resolving ocean model, *Geosci. Model Dev.*, 6, 591–615, doi:10.5194/gmd-6-591-2013, 2013.

Prasanna Kumar, S., Divya David, T., Byju, P., Narvekar, J., Yoneyama, K., Nakatani, N., Ishida, A., Horii, T., Masumoto, Y., and Mizuno, K.: Bio-physical coupling and ocean dynamics in the central equatorial Indian Ocean during 2006 Indian Ocean Dipole, *Geophys. Res. Lett.*, 39, L14601, doi:10.1029/2012GL052609, 2012.

Ridgway, K. R., Dunn, J. R., and Wilkin, J. L.: Ocean interpolation by four-dimensional weighted least squares – application to the waters around Australasia, *J. Ocean. Atmos. Tech.*, 19, 1357–1375, 2002.

Biogeochemical variability in the equatorial Indian Ocean

P. G. Strutton et al.

Title Page

Abstract

Introduction

Conclusions

References

Tables

Figures

⏪

⏩

◀

▶

Back

Close

Full Screen / Esc

Printer-friendly Version

Interactive Discussion

- Roemmich, D. and Gilson, J.: The 2004–2008 mean and annual cycle of temperature, salinity, and steric height in the global ocean from the Argo program, *Prog. Oceanogr.*, 82, 81–100, doi:10.1016/j.pocean.2009.03.004, 2009.
- 5 Saji, N. H., Goswami, B. N., Vinayachandran, P. N., and Yamagata, T.: A dipole in the tropical Indian Ocean, *Nature*, 401, 360–363, 1999.
- Schott, F. and McCreary, J. P.: The monsoon circulation of the Indian Ocean, *Prog. Oceanogr.*, 51, 1–123, 2001.
- Schott, F. A., Xie, S.-P., and McCreary Jr., J. P.: Indian Ocean circulation and climate variability, *Rev. Geophys.*, 47, RG1002, doi:10.1029/2007RG000245, 2009.
- 10 Sengupta, D., Senan, R., Murty, V. S. N., and Fernando, V.: A biweekly mode in the equatorial Indian Ocean, *J. Geophys. Res.*, 109, C10003, doi:10.1029/2004JC002329, 2004.
- Shinoda, T.: Observation of first and second baroclinic mode Yanai waves in the ocean, *Q. J. Roy. Meteor. Soc.*, 138, 1018–1024, 2012.
- Vinayachandran, P. N. and Nanjundiah, R. S.: Indian Ocean sea surface salinity variations in a coupled model, *Clim. Dynam.*, 33, 245–263, 2009.
- 15 Wiggert, J. D., Murtugudde, R. G., and Christian, J. R.: Annual ecosystem variability in the tropical Indian Ocean: results of a coupled bio-physical ocean general circulation model, *Deep-Sea Res. Pt. II* 53, 644–676, 2006.
- Wyrtki, K.: An equatorial jet in the Indian Ocean, *Science*, 181, 262–264, 1973a.
- 20 Wyrtki, K.: Physical oceanography of the Indian Ocean, in: *The Biology of the Indian Ocean*, edited by: Zeitschel, B., Springer-Verlag, Berlin, 18–36, 1973b.
- Yanai, M. and Maruyama, T.: Stratospheric wave disturbances propagating over the equatorial Pacific, *J. Meteorol. Soc. Jpn.*, 44, 291–294, 1966.

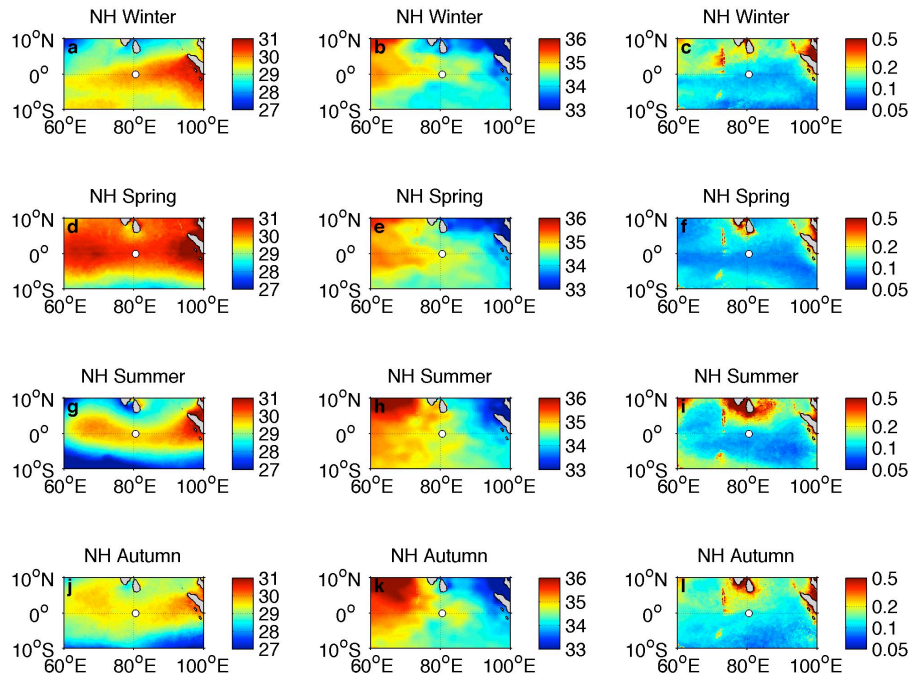


Fig. 1. The seasonal climatology of SST (left column of panels), salinity (center column) and chlorophyll (right column) for a region of the Indian Ocean encompassing the RAMA mooring at the equator, 80.5° E. SST and chlorophyll data sets are from the MODIS Aqua satellite at 9 km spatial resolution. Salinity data are from the CSIRO Atlas of Regional Seas (CARS: <http://www.marine.csiro.au/~dunn/cars2009/>). The seasons are defined as follows: boreal winter 21 December to 21 March, spring 21 March to 20 June, summer 21 June to 21 September, autumn 21 September to 21 December. The seasonal climatology illustrates the potential for salty, high chlorophyll waters to be advected into the vicinity of the mooring in boreal autumn.

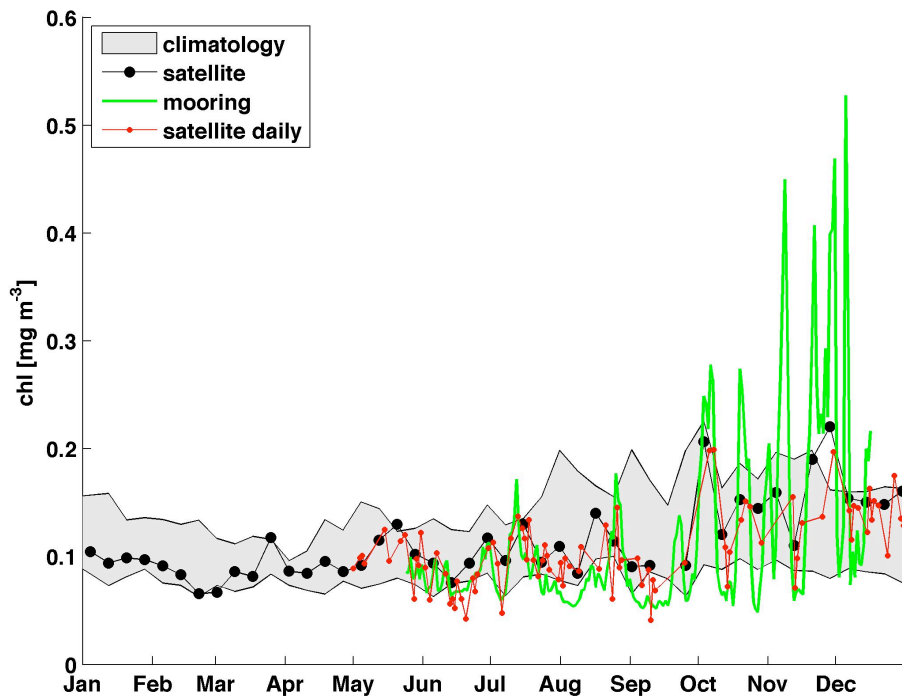


Fig. 2. Chlorophyll concentrations at the mooring location. The grey shading indicates the mean annual cycle \pm one standard deviation based on SeaWiFS and MODIS Aqua 8 day satellite chlorophyll for the period 1998 to 2012. The filled black circles are merged SeaWiFS/MODIS Aqua 8 day chlorophyll for 2010, the green line is the daily averaged 20 m in situ FLNTU chlorophyll and the red line is a 3 day smoothing of daily satellite data for 2010. The satellite data are averaged from all valid pixels in a 1° (111 km) square around the mooring location.

Biogeochemical variability in the equatorial Indian Ocean

P. G. Strutton et al.

[Title Page](#)

[Abstract](#) [Introduction](#)

[Conclusions](#) [References](#)

[Tables](#) [Figures](#)

[◀](#) [▶](#)

[◀](#) [▶](#)

[Back](#) [Close](#)

[Full Screen / Esc](#)

[Printer-friendly Version](#)

[Interactive Discussion](#)



Biogeochemical
variability in the
equatorial Indian
Ocean

P. G. Strutton et al.

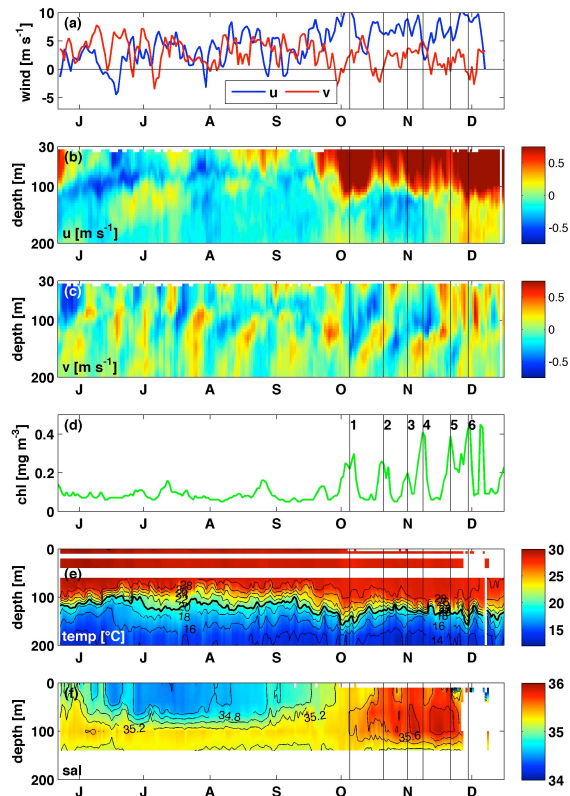


Fig. 3. Time series of mooring physical and biological parameters. **(a)** Zonal [u , ms^{-1}] and meridional [v , ms^{-1}] winds; **(b)** zonal [u , ms^{-1}] current; **(c)** meridional [v , ms^{-1}] current; **(d)** chlorophyll concentration [mg m^{-3}] from the moored fluorometer; **(e)** temperature [T , $^{\circ}\text{C}$] with 20°C contour in bold; **(f)** salinity. Gaps in the T and S data are due to sensor failure. Vertical black lines in each panel indicate the 6 main chlorophyll peaks during October to December, which are numbered in panel **(d)**.

Biogeochemical
variability in the
equatorial Indian
Ocean

P. G. Strutton et al.

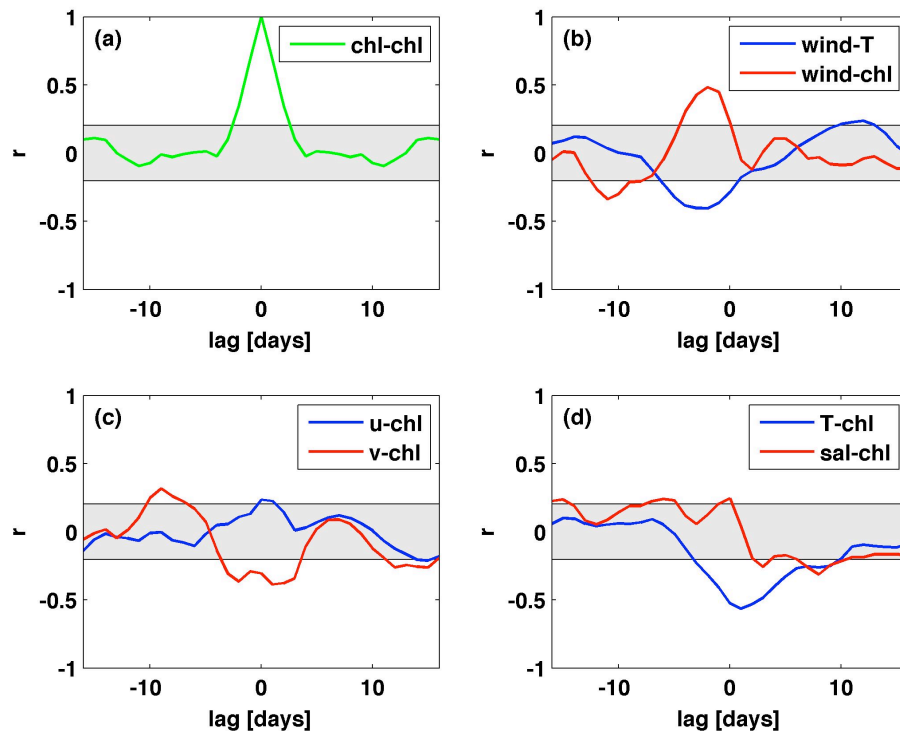


Fig. 4. Cross-correlation analyses of physical parameters and chlorophyll from the RAMA mooring at 80.5° E, 0°. In the figure legends, the first-named parameter leads the second-named, so, for example, the strong positive peak in wind speed and chl in panel (b) means that stronger winds are followed by increased chlorophyll about 2–3 days later. The cross-correlation analysis was performed for the section of the data set where the chlorophyll spikes were most obvious: 15 September 2010 to 15 December 2010. The shaded region in each panel indicates the 95 % confidence interval.

Title Page

Abstract

Introduction

Conclusions

References

Tables

Figures

⏪

⏩

◀

▶

Back

Close

Full Screen / Esc

Printer-friendly Version

Interactive Discussion

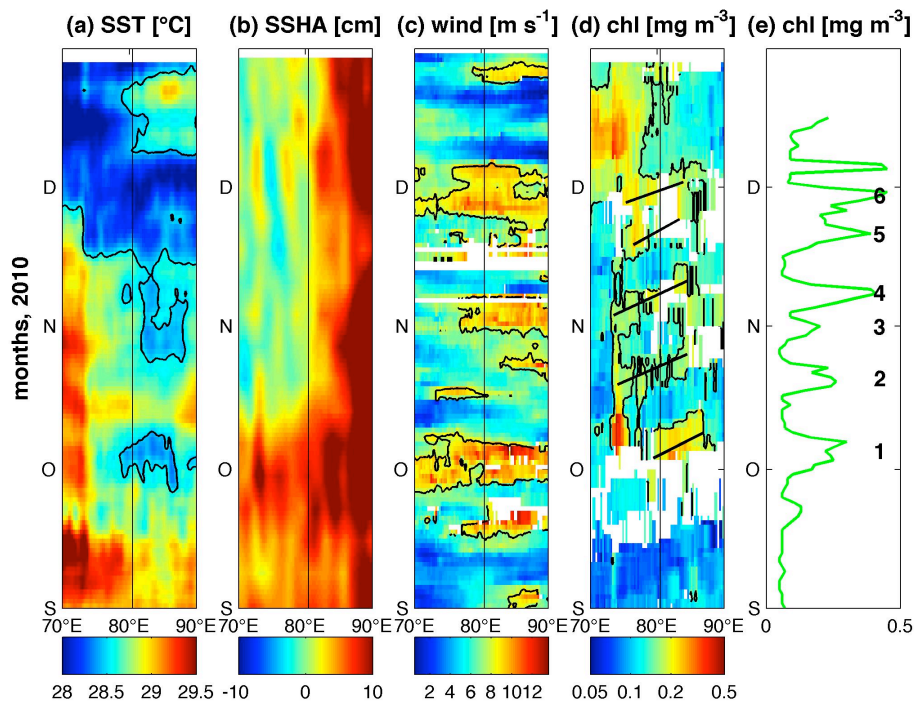


Fig. 5. Hovmuller plots of remotely sensed observations along the equator centered at the mooring location: **(a)** Microwave optimally interpolated SST; **(b)** SSH anomaly from AVISO; **(c)** wind speed from WindSat; and **(d)** satellite chlorophyll from MODIS and SeaWiFS combined. Panel **(e)** is the fluorometer time series from the mooring, at 25 m depth. Black contours in the Hovmuller plots are 28.5°C in **(a)**, 8 m s^{-1} in **(c)**, and 0.15 mg m^{-3} in **(d)**. The solid lines in **(d)** are intended to track eastward migrating chlorophyll maxima. The numbers in **(e)** indicate 6 major chlorophyll peaks observed at the mooring. Peak 3 and the peak in early December were not visible in the satellite data so no slope was calculated for these events.

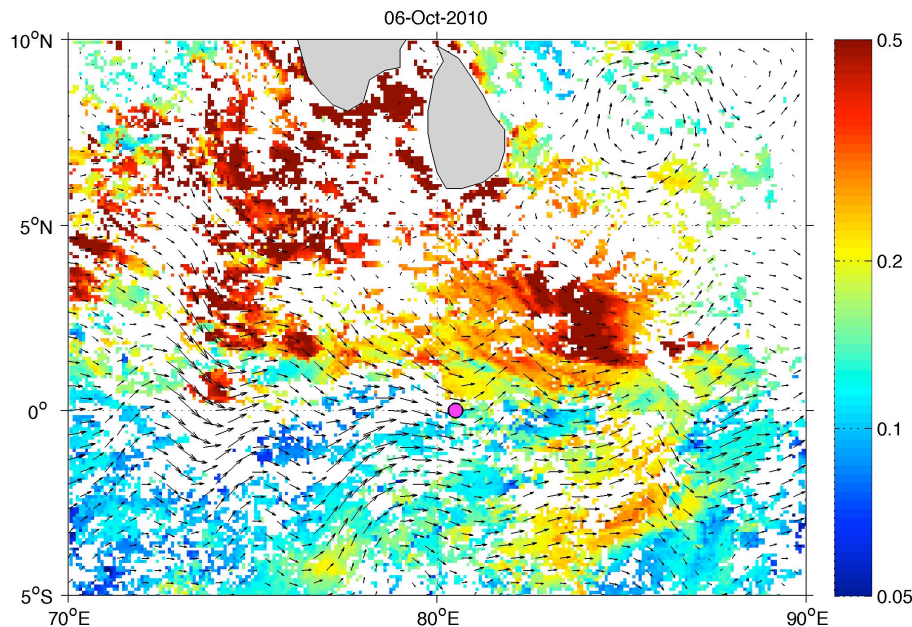


Fig. 6. Chlorophyll map created from a 15 day average of MODIS Aqua data centered on 6 October 2010, peak 1 in Fig. 5. The mooring on the equator at 80.5° E is marked with a magenta circle. Vectors are OSCAR geostrophic currents calculated from satellite altimetry and scatterometry for a 5 day period centered on 1 October 2010. The figure illustrates the high chlorophyll from the Maldives (~ 73° E) being advected eastwards by the large-scale flow and southwards towards the mooring by wave processes.

**Biogeochemical
variability in the
equatorial Indian
Ocean**

P. G. Strutton et al.

Title Page

Abstract

Introduction

Conclusions

References

Tables

Figures

⏪

⏩

◀

▶

Back

Close

Full Screen / Esc

Printer-friendly Version

Interactive Discussion

Biogeochemical
variability in the
equatorial Indian
Ocean

P. G. Strutton et al.

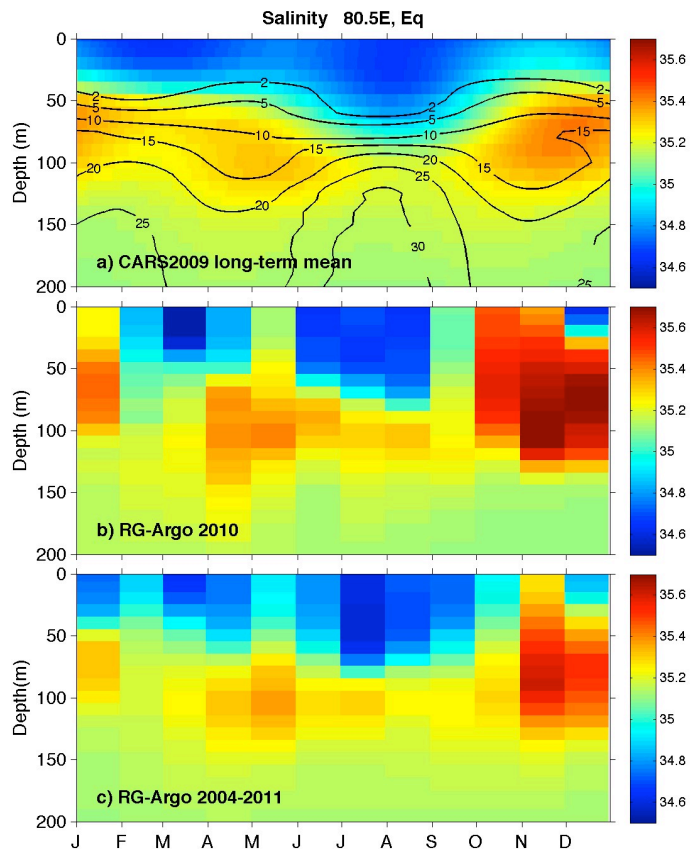


Fig. 7. Time-depth sections of salinity (PSS-78) for the mooring location. **(a)** The long term mean from CARS with nitrate [mmol m^{-3}], also from CARS contoured; **(b)** the RG-Argo product for 2010; **(c)** the RG-Argo climatology based on data from 2004 to 2011.

Title Page

Abstract

Introduction

Conclusions

References

Tables

Figures

◀

▶

◀

▶

Back

Close

Full Screen / Esc

Printer-friendly Version

Interactive Discussion

**Biogeochemical
variability in the
equatorial Indian
Ocean**

P. G. Strutton et al.

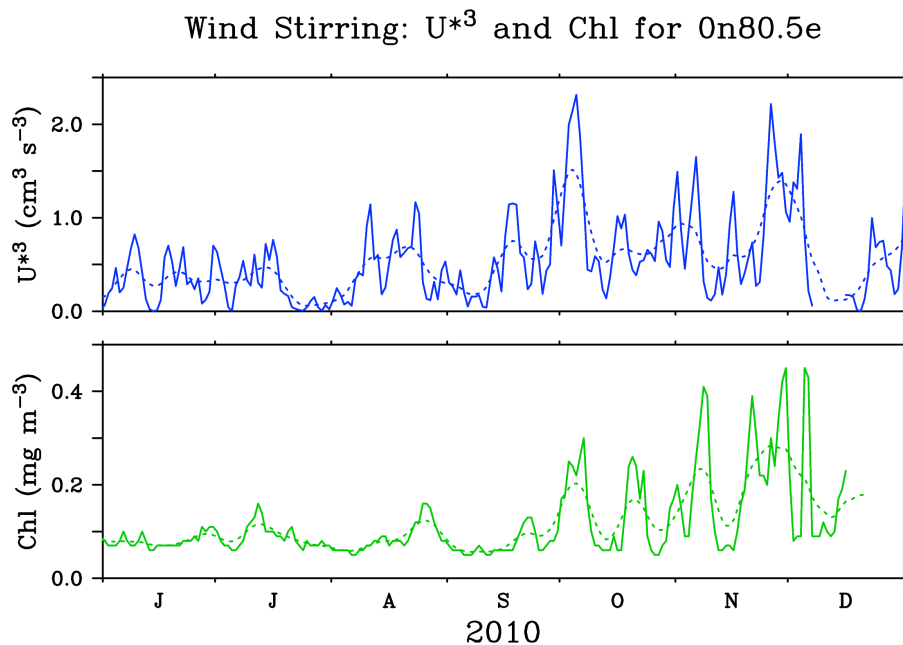


Fig. 8. A closer look at winds and chlorophyll at the mooring location. Top panel is the cube of wind speed [$\text{cm}^3 \text{s}^{-3}$], which is a measure of wind-induced turbulence. Bottom panel is the mooring chlorophyll fluorescence measurements [mg m^{-3}]. Dashed lines are a one-week moving average filter.

[Title Page](#)[Abstract](#)[Introduction](#)[Conclusions](#)[References](#)[Tables](#)[Figures](#)[⏪](#)[⏩](#)[◀](#)[▶](#)[Back](#)[Close](#)[Full Screen / Esc](#)[Printer-friendly Version](#)[Interactive Discussion](#)

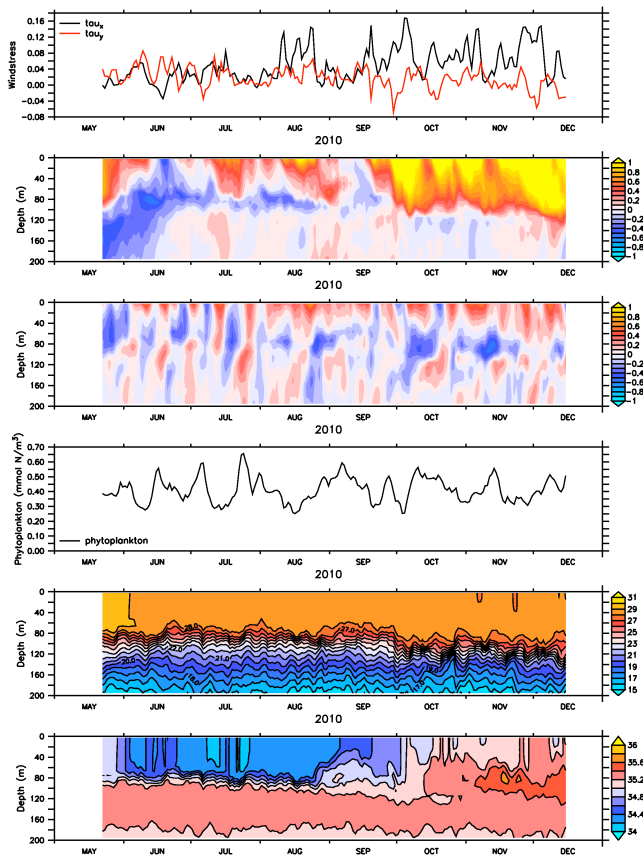


Fig. 9. Simulation of parameters at the mooring site from OFAM3 model output. Panels from top to bottom: zonal (black) and meridional (red) components of wind stress [N m^{-2}]; zonal current velocity [m s^{-1}]; meridional current velocity [m s^{-1}]; phytoplankton [mmol N m^{-3}]; temperature [$^{\circ}\text{C}$]; salinity [PSS-78].

Biogeochemical
variability in the
equatorial Indian
Ocean

P. G. Strutton et al.

Title Page

Abstract Introduction

Conclusions References

Tables Figures

◀ ▶

◀ ▶

Back Close

Full Screen / Esc

Printer-friendly Version

Interactive Discussion



BGD

11, 6185–6219, 2014

Biogeochemical variability in the equatorial Indian Ocean

P. G. Strutton et al.

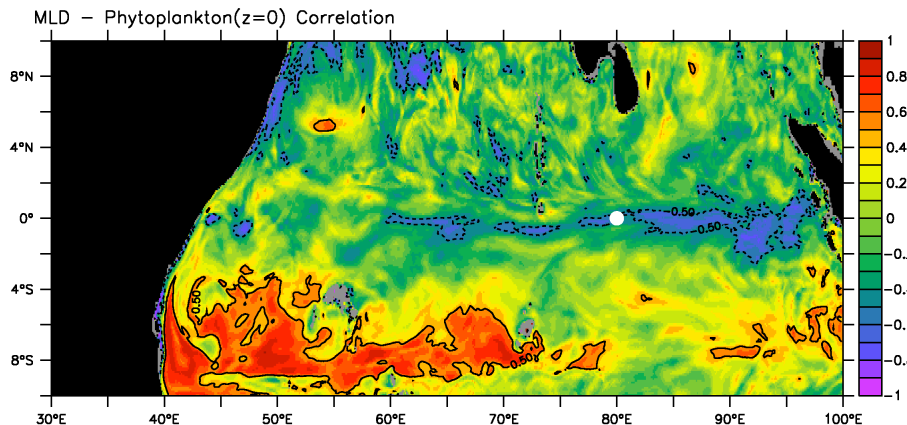


Fig. 10. The correlation between mixed layer depth and phytoplankton concentration in the OFAM3 model. The mooring is marked with a white circle.

[Title Page](#)[Abstract](#)[Introduction](#)[Conclusions](#)[References](#)[Tables](#)[Figures](#)[Back](#)[Close](#)[Full Screen / Esc](#)[Printer-friendly Version](#)[Interactive Discussion](#)